AGU PUBLICATIONS

Journal of Advances in Modeling Earth Systems

RESEARCH ARTICLE

10.1002/2017MS001035

Key Points:
- The original ZM scheme has poor resolution adaptability, double counting convective adjustment as the resolution increases
- Applying spatial and temporal averaging to the CAPE tendency in the closure scheme improves resolution adaptability of the ZM scheme
- The averaging algorithm improves both the overall magnitude and the distribution of total precipitation at high resolutions

Correspondence to:
Y. Yun,
yunyx@cma.gov.cn

Citation:
Yun, Y., Fan, J., Xiao, H., Zhang, G. J., Ghan, S. J., Xu, K.-M., . . . Gustafson, W. I. (2017). Assessing the resolution adaptability of the Zhang-Mcfarlane cumulus parameterization with spatial and temporal averaging. *Journal of Advances in Modeling Earth Systems*, *9*, 2753–2770. https://doi.org/10.1002/2017MS001035

Received 3 MAY 2017
Accepted 30 OCT 2017
Accepted article online 3 NOV 2017
Published online 30 NOV 2017

Assessing the Resolution Adaptability of the Zhang-McFarlane Cumulus Parameterization With Spatial and Temporal Averaging

Yuxing Yun[1,2], Jiwen Fan[1], Heng Xiao[1], Guang J. Zhang[3], Steven J. Ghan[1], Kuan-Man Xu[4], Po-Lun Ma[1], and William I. Gustafson Jr.[1]

[1]Atmospheric Sciences and Global Change Division, Pacific Northwest National Laboratory, Richland, WA, USA, [2]State Key Laboratory of Severe Weather, Chinese Academy of Meteorological Sciences, Beijing, China, [3]Scripps Institution of Oceanography, University of California, San Diego, CA, USA, [4]NASA Langley Research Center, Hampton, VA, USA

Abstract With increasing computational capabilities, cumulus parameterizations that are adaptable to the smaller grid spacing and temporal interval for high-resolution climate model simulations are needed. In this study, we propose a method to improve the resolution adaptability of the Zhang-McFarlane (ZM) scheme, by implementing spatial and temporal averaging to the CAPE tendency. This method allows for a more consistent application of the quasi-equilibrium (QE) hypothesis at high spatial and temporal resolutions. The resolution adaptability of the original ZM scheme, the scheme with spatial averaging, and the scheme with spatiotemporal averaging at 4–32 km grid spacings are assessed using the Weather Research and Forecasting (WRF) model by comparing to cloud resolving model (CRM) simulation results coarse-grained to these same grid spacings. We show the original ZM scheme has poor resolution adaptability, with spatiotemporally averaged subgrid convective transport and convective precipitation increasing significantly as the resolution increases. The spatial averaging method improves the resolution adaptability of the ZM scheme and better conserves total transport and total precipitation. Temporal averaging further improves the resolution adaptability of the scheme. With better constrained (although smoothed) convective transport and precipitation, both the spatial distribution and time series of total precipitation at 4 and 8 km grid spacings are improved with the averaging methods. The results could help develop resolution adaptability for other cumulus parameterizations that are based on the QE assumption.

1. Introduction

Cumulus convection has long been a central issue in atmospheric modeling (Arakawa, 2004). Since the typical grid spacing (∼100 km) of general circulation models (GCMs) is too coarse to simulate the dynamics of cumulus clouds, cumulus convection is parameterized as a subgrid-scale process. However, owing to the development of computational capabilities, the newest generation of GCMs are now designed to run at higher resolutions (∼25 km grid spacing), with regional refinement to a few kilometer grid spacings. The small grid spacings may invalidate some assumptions used in traditional cumulus parameterizations, because they are only justified at much coarser scales (the spatial and temporal scale of traditional GCMs) (Arakawa & Wu, 2013). Therefore, it is imperative to develop resolution adaptable (also referred to as resolution aware, resolution-dependent, or scale aware) cumulus parameterizations that can adapt to the change in model resolution and give accurate results up to resolutions of a few kilometers.

The majority of cumulus parameterization schemes are based on variations of the quasi-equilibrium (QE) assumption (Arakawa & Jung, 2011; Kain & Fritsch, 1990; Moorthi & Suarez, 1992; Plant & Craig, 2008; Zhang & McFarlane, 1995). The QE assumption was originally proposed by Arakawa and Schubert (1974) (AS74) as follows: for a horizontal area large enough to contain an ensemble of cumulus clouds, if the time scale of convective adjustment is much shorter than that of the large-scale processes, the cumulus ensemble goes through a series of quasi-equilibria with the concurrent large-scale forcing as the cumulus ensemble acts to remove the destabilization generated by the large-scale forcing.

In convective parameterizations, the QE assumption is usually expressed in terms of convective available potential energy (CAPE or A). The time derivative of A, i.e., the generation or destruction of CAPE, can be expressed as

$$\frac{dA}{dt}=\left(\frac{dA}{dt}\right)_{LS}+\left(\frac{dA}{dt}\right)_{CU}. \tag{1}$$

Here the first and second terms on the right-hand side of (1) represent the CAPE change due to large-scale and convective processes, respectively. The large-scale processes include temperature and moisture advection, radiative heating, and surface heat and moisture fluxes (Zhang, 2003).

Under the quasi-equilibrium condition, we have

$$\left|\frac{dA}{dt}\right| \ll \left|\left(\frac{dA}{dt}\right)_{LS}\right|, \; and \; \left|\frac{dA}{dt}\right| \ll \left|\left(\frac{dA}{dt}\right)_{CU}\right|. \tag{2}$$

Therefore

$$-\left(\frac{dA}{dt}\right)_{CU} \approx \left(\frac{dA}{dt}\right)_{LS}. \tag{3}$$

Equation (3) states that the stabilization of the atmosphere by cumulus convection is approximately balanced by the destabilization of the atmosphere by large-scale processes. Equation (3) expresses a negative feedback to large-scale destabilization, which is often called “adjustment” (Arakawa, 2004). Some parameterizations have also used “relaxed adjustment,” in which the convective adjustment given by the left-hand side of equation (3) is relaxed to a fraction of the large-scale forcing on the right-hand side (Kain & Fritsch, 1990; Moorthi & Suarez, 1992).

As mentioned above, QE assumes both spatial and temporal separation of scales between convective elements and the so-called large-scale (or grid-scale in the context of GCMs) processes. There have been many debates about whether and where such a separation of scales really exists and whether QE applies in a deterministic-mechanistic or statistical sense (see, e.g., Arakawa, 2004; Jones & Randall, 2011; Mapes, 1997; Neelin et al., 2008; Raymond & Herman, 2011; Yano & Plant, 2012, and references therein). Our current interpretation of QE is more from a statistical point of view and similar to the law of large numbers in statistical mechanics (see also Plant & Craig, 2008; Williams, 2005), which requires a separation between the horizontal scale of convective elements and that of the grid box to allow for the parameterization (both statistically and physically, see also Arakawa, 2004) of a large ensemble of convective elements. But with decreasing grid spacing in newer-generation GCMs, it is obvious that such a separation of scales ceases to exist.

Recently, there have been considerable efforts in developing and modifying convection parameterizations for smaller grid spacing (Arakawa & Wu, 2013; Gerard et al., 2009; Grell & Freitas, 2014; Park, 2014; Xiao et al., 2015). Gerard et al. (2009) and Park (2014) both proposed new parameterizations that are not based on the QE assumption. For QE-based schemes, Arakawa and Wu (2013) proposed a way to solve this problem by scaling down the subgrid convective transport (convective transport that cannot be resolved by grid-scale motion and needs to be parameterized, referred to as “convective transport” hereafter) for fine resolutions, by using a diagnosed convective updraft fraction. Grell and Freitas (2014) applied a modified version of Arakawa and Wu (2013) in their convection parameterization. However, Zhang et al. (2015) argued that increased convective updraft fraction at smaller grid spacing is not the cause of the convective transport problem. Xiao et al. (2015) (Xiao15) proposed another method to improve resolution adaptability for QE-based schemes by applying the closure not on the local grid box, but on an area surrounding the local grid box that is large enough to apply the QE assumption, e.g., 128×128 km^2. They tested this method in an offline study with one of the QE-based convective parameterizations, namely the Zhang and McFarlane (1995) (ZM) scheme, and found the diagnosed resolution adaptability significantly improved with this new algorithm. We take a step further here to do an online, fully interactive test of the method. The online approach takes into account the important feedback processes that happen between the physics and dynamics, which could not be captured in the offline analysis of Xiao15. Moreover, we also implement an additional temporal averaging method on top of spatial averaging, which further improves the resolution adaptability and also allows for more consistent application of the original QE concept at high spatial and temporal resolutions.

The ZM scheme is widely used in both global and regional climate models. In this study, we will use the ZM deep convection scheme as the target for assessment. Since the Weather Research and Forecasting (WRF) model can be easily set up to run at different resolutions, we will use the WRF model as our test bed. We will assess the resolution adaptability of the original ZM scheme, the ZM scheme with the spatial averaging method in Xiao15, as well as the ZM scheme with a combined spatial and temporal averaging method. Section 2 briefly describes the methods and experiments. Section 3 discusses the resultant change to the resolution adaptability of convective transport of moist static energy (MSE) and convective precipitation, and also evaluates the spatial distribution and time series of precipitation. Summary and discussion of implications are given in the last section.

2. Methods and Experiments

2.1. The Zhang-McFarlane Deep Convection Scheme

The ZM scheme is based on a plume ensemble concept and utilizes the QE assumption to construct a bulk representation of the effect of the cumulus ensemble. ZM further assumes that the ensemble of plumes acts to relax the atmosphere to a state of neutral buoyancy.

The original closure condition of the ZM scheme is a variant of equation (3):

$$M_b F = \frac{\max\,(A - A_0,\ 0)}{\tau}, \tag{4}$$

where M_b is the cloud-base mass flux. F is the rate of CAPE consumption per unit M_b, calculated by the scheme's plume model. A_0 is the CAPE of the "equilibrium state," an empirical constant. τ is also an empirical constant representing the convective adjustment time scale. Here, deep convection can only be triggered when $A > A_0$, and CAPE is consumed by cumulus convection at an exponential rate with characteristic time scale τ. The left-hand side of equation (4) can be seen as a representation of $-(dA/dt)_{CU}$ in equation (3), and likewise, the right-hand side can be seen as a simple approximation to $(dA/dt)_{LS}$.

Later, a modified closure scheme that directly calculates $(dA/dt)_{LS}$ was proposed in (Zhang, 2002):

$$M_b F = \left(\frac{dA}{dt}\right)_{LS+} = \max\left[\left(\frac{dA}{dt}\right)_{LS},\ 0\right], \tag{5}$$

where $(dA/dt)_{LS+}$ is the positive definite of $(dA/dt)_{LS}$. In this new version, convection is triggered only when there is a positive change of CAPE ($(dA/dt)_{LS} > 0$).

In ZM, a plume model calculates the vertical profile of convective transport assuming $M_b = 1$, which is equal to the convective transport per unit M_b. Then, M_b, i.e., the cloud-base mass flux (calculated from equations (4) or (5)), is used to convert the per unit transport profile to the actual profile.

2.2. The Spatial and Temporal Averaging Methods Implemented in the ZM Scheme

Xiao15 compared the resolution dependence of $(dA/dt)_{LS+}$ (diagnosed using output from a cloud resolving model (CRM) simulation coarsened to different spatial resolutions) to that of the convective transport calculated by the ZM scheme (using the same coarsened CRM output as input) and found both of them decrease only slightly, or even increase, with increasing resolution in terms of spatiotemporal mean. This shows that for the ZM scheme, $(dA/dt)_{LS+}$ dictates the resolution adaptability of the convective transport through the determination of M_b in equation (5). The mean $(dA/dt)_{LS}$ itself (without taking positive definite), on the other hand, shows a significant decrease with increasing resolution, similar to the decrease of the mean convective transport directly diagnosed from the CRM (Figure 5 and Figure 4(b) in Xiao15). Xiao15 suggested that (1) the mean $(dA/dt)_{LS}$ decreases simply because the resolved circulation (i.e., grid-scale advection) becomes more stabilizing (i.e., destroys more CAPE) with increasing resolution; and (2) the decrease of mean convective transport (diagnosed from CRM output) is also the consequence of the increase in the overall strength (in terms of either vertical transport or destruction of CAPE) of the resolved circulation. But, at smaller grid spacings, the frequency distribution of $(dA/dt)_{LS}$ calculated in the local grid boxes becomes broader and the chances of finding extreme values of $(dA/dt)_{LS}$ increases, leading to an increase in the difference between the spatiotemporal mean values of $(dA/dt)_{LS}$ and $(dA/dt)_{LS+}$. This suggests that applying the QE-based closure (i.e., equation (5)) locally not only violates the presumptions of QE but also leads to underestimation of the decrease of mean convective transport with increasing resolution and masks the resolution dependence of $(dA/dt)_{LS}$.

To remedy this, Xiao15 proposed a simple modification to equation (5). Instead of using the $(dA/dt)_{LS}$ calculated in the local grid box, they used a spatial average of $(dA/dt)_{LS}$ over a large area (128×128 km^2) centered on the local grid box. This new area-averaged large-scale forcing is denoted as $\overline{\overline{(dA/dt)}}_{LS}$. Therefore, the closure scheme becomes:

$$M_b F = \overline{\overline{\left(\frac{dA}{dt}\right)}}_{LS+} = \max\left[\overline{\overline{\left(\frac{dA}{dt}\right)}}_{LS}, 0\right]. \tag{6}$$

This modification basically prevents triggering of convection based on the local grid box values of $(dA/dt)_{LS}$ at high resolutions and allows for consistent application of the QE-based closure at the spatial scales it is designed for. Xiao15 showed in their diagnostic analysis that this modification leads to improved resolution dependence of convective transport in terms of spatiotemporal averages. The current study implements this method, and advances over the earlier study by doing the tests using an online, fully interactive version of the modified ZM that permits the model to respond to the improved application of the QE-based closure.

When the dynamic time step becomes small at high resolutions, calculating $(dA/dt)_{LS}$ in a single time step and using it in equation (5) is in contradiction with the presumed scale separation in time for the QE-based closure (AS74, Neelin et al., 2008). In this study, we propose to test an additional temporal averaging method to $(dA/dt)_{LS}$ that can allow for more consistent application of the original QE concept at high spatial and temporal resolutions: Instead of using $(dA/dt)_{LS}$ calculated at the current time step, we use the averaged $(dA/dt)_{LS}$ over a longer time scale (prior to the current time step) in the closure scheme. The offline study in Xiao15 applied it by using the $(dA/dt)_{LS}$ diagnosed from a CRM at the same 10 min frequency for grid spacings from 8 to 256 km. The good resolution dependence of the resultant convective transport suggests that 10 min is a practical choice for the time averaging period. It also allows for a consistent comparison with results from Xiao15.

2.3. Model and Experiments

The model used here is the WRF model version 3.6.1 configured to use the Community Atmosphere Model version 5.1 (CAM5) physics suite (Ma et al., 2014). Simulations with the ZM scheme are performed at four horizontal grid spacings (4, 8, 16, and 32 km). The horizontal simulation domain is $1,280 \times 1,280$ km^2 over the tropical western Pacific, with the inner $1,024 \times 1,024$ km^2 used for analysis. The vertical coordinate has 41 levels with variable resolution (60.12 m at the lowest level to 604.7 m at the highest level). The simulation time is 18–26 January 2006, which is during the active monsoon period from the Tropical Warm Pool-International Cloud Experiment (TWP-ICE) field campaign (May et al., 2009), with results from 00:00 UTC on 19 January to 16:00 UTC on 24 January used for analysis. We select this period for analysis because it is after the model is fully initialized, and before it starts to diverge significantly from observation. It also captures the major precipitation events. The time step is 10, 20, 50, and 100 s for horizontal grid spacings of 4, 8, 16, and 32 km, respectively. Instantaneous fields are written out every 30 min. The lateral and lower boundary conditions are supplied by National Center for Environmental Prediction (NCEP) Final (FNL) reanalysis data. We use the Morrison 2-moment scheme (Morrison et al., 2005) for microphysics, the Rapid Radiative Transfer Model for General Circulation Models (RRTMG) (Iacono et al., 2000) for short-wave and long-wave radiation, and the University of Washington scheme (Bretherton & Park, 2009) for PBL and shallow convection in the model.

Table 1
Description of Experiments

	Description
originalZM	Use the original $(dA/dt)_{LS}$ with no averaging
avgspace	Apply only spatial averaging for $(dA/dt)_{LS}$
avgspace_time	Apply both spatial and temporal averaging for $(dA/dt)_{LS}$
1km_CRM	1km resolution CRM run, with cumulus scheme turned off

Note. The first three sets of experiments consist of four simulations performed with 4, 8, 16, and 32 km horizontal grid spacings.

Table 1 summarizes the three sets of experiments we designed with the ZM scheme to test the resolution adaptability of the scheme with the proposed spatial and temporal averaging. Each set of experiments consists of four simulations performed with 4, 8, 16, and 32 km horizontal grid spacings. The "originalZM" experiments use the ZM scheme, with the positive-definite grid-scale tendency of CAPE ($(dA/dt)_{LS+}$) calculated at the local grid column for the closure scheme (equation (5)), following (Zhang, 2002).

Experiments "avgspace" are based on originalZM, but, instead of using the $(dA/dt)_{LS}$ computed at the local grid column, it uses the averaged $(dA/dt)_{LS}$ of a large area centered on the local grid column ($\overline{(dA/dt)_{LS}}$). The averaging area used in this study is about 90 × 90 km^2 in size and is slightly different among simulations with different resolutions, since we need to include whole grid cells and the target grid cell needs to be in the center of the area. Xiao15 has found minimal sensitivity to the size of the averaging area ranging from 64 × 64 to 256 × 256 km^2. No special treatment is given to grid columns whose averaging area includes both land and ocean. In this set of experiments, $(dA/dt)_{LS}$ is calculated at the respective dynamical time step for each horizontal resolution.

Experiments "avgspace_time" apply both spatial and temporal averaging to $(dA/dt)_{LS}$. In this set of experiments, $(dA/dt)_{LS}$ is averaged over 10 min. The dynamical time step is unchanged. This set of experiments makes the spatial and temporal scales at which $(dA/dt)_{LS}$ is calculated more suitable for applying the QE assumption regardless of model resolution. In this online experiment, we only have information of $(dA/dt)_{LS}$ in the past 10 min at the current time step. This introduces a small lag between the time averaged $(dA/dt)_{LS}$ and the parameterized convection, which is different from the offline test in Xiao15 where information from both the "past" and the "future" are used in the 10 min time averaging. Judging from results of the online experiments presented below, this lag does not affect the overall behavior of the averaging algorithms. We have also tried using a 20 min averaging time scale for 8, 16, and 32 km grid spacings. The results show that resolution dependence has little sensitivity to this change in the averaging time scale.

To evaluate the aforementioned experiments, we also performed a benchmark 1 × 1 km^2 grid spacing CRM simulation with WRF (1km_CRM in Table 1). This grid spacing has been shown to resolve deep convective cloud systems reasonably well (Lee et al., 2008; Tao, 2007). In this simulation, both deep and shallow convection schemes are turned off and the time step is 3 s. The precipitation time series (Figure 1) and map of accumulated precipitation (Figure 2) from the CRM run are compared to observations from TRMM. The CRM output is averaged to match the spatial and temporal resolutions of TRMM data (3 hourly, 0.25 × 0.25 degree). The CRM run captures the timing of maximum precipitation, but overpredicts the accumulated precipitation.

2.4. Diagnosing Convective Transport and Precipitation From CRM

The results from the 1km_CRM run are used to diagnose convective, resolved, and total transport of MSE for a series of subdomain sizes from 4, 8, 16, to 32 km using the same method as Arakawa and Wu (2013). Convective transport of MSE in a subdomain is calculated as:

$$\rho\overline{w'h'} = \rho\frac{1}{N}\sum_{i=1}^{N}(w_i-\bar{w})\left(h_i-\bar{h}\right), \tag{7}$$

where ρ is the air density, w_i and h_i are the vertical velocity and moist static energy at each CRM grid box i in the subdomain, and N is the number of CRM grid boxes in the subdomain. The overbar and prime represent the mean over the subdomain and the deviation from it, respectively. Following Liu et al. (2015), updrafts are identified by: (1) vertical velocities $(w) > 1$ m s^{-1} and total hydrometer mixing ratio $(Q_{tot}) > 1 \times 10^{-5}$ kg kg^{-1} or (2) $w > 2$ m s^{-1}. Downdrafts are identified by $w < -1$ m s^{-1} and $Q_{tot} > 1 \times 10^{-5}$ kg kg^{-1}. More details about diagnosing convective transport of MSE from CRM results can be found in Liu et al. (2015). In the simulations with the ZM scheme, convective transport of MSE is calculated online as:

$$m_u\left(h_u-\bar{h}\right)+m_d\left(h_d-\bar{h}\right), \tag{8}$$

where m_u/m_d are the updraft/downdraft mass flux, h_u/h_d are the updraft/downdraft MSE, and $\bar{h}$ is the grid mean MSE.

Resolved transport of MSE is calculated as the deviation of subdomain or grid averaged mass flux and MSE from the domain averaged values (Arakawa & Wu, 2013), $(\bar{m}-\hat{m})(\bar{h}-\hat{h})$, where $\bar{m}$ is the subdomain-averaged mass flux and $\hat{m}$ and $\hat{h}$ are the domain averaged mass flux and MSE, respectively. The sum of convective and resolved transport of MSE is then the total transport of MSE.

We also partition the precipitation from the CRM run into subgrid convective and resolved portions relative to each subdomain area. To do

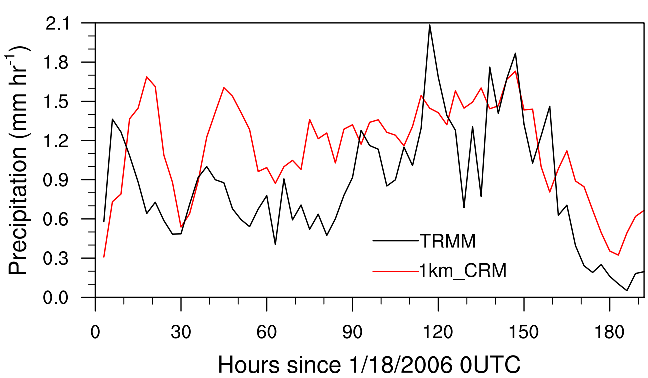

Figure 1. Time series of domain averaged precipitation (mm h^{-1}) from 1km_CRM and TRMM.

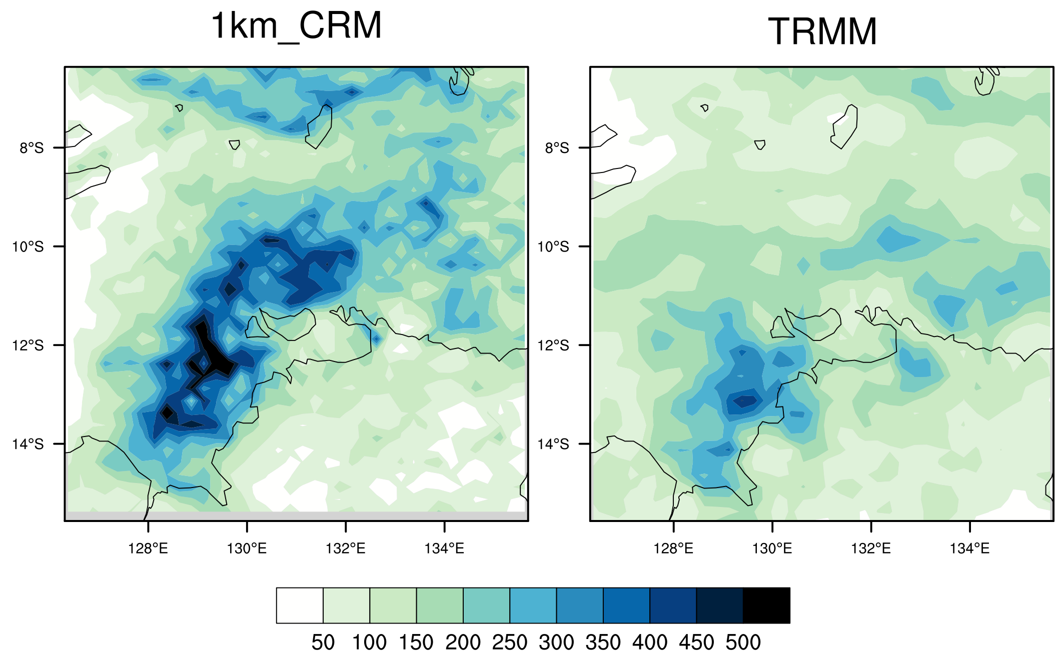

Figure 2. Accumulated precipitation (mm) from 1km_CRM and TRMM over the 136 h analysis period.

so, we first use the radar reflectivity from model output to classify the precipitation into either convective or stratiform for every CRM grid point, using the difference between the radar reflectivity of the grid point and the mean background reflectivity within an 11 km radius, as described in Steiner et al. (1995).

Then for each subdomain, if there are both convective and stratiform precipitation as classified by the Steiner method, we assume all convective precipitation belongs to the subgrid category. However, if the precipitation of every CRM grid point within the subdomain is classified as convective by the Steiner method, which happens more often for smaller subdomain sizes, we need to examine the heterogeneity of the convective precipitation within the subdomain to determine how much precipitation should be considered as subgrid convective precipitation. To do so, we compare the precipitation in each CRM grid point to the subdomain-averaged precipitation. If the precipitation for the CRM grid point is larger than 3 times the subdomain-averaged value, then it is considered highly heterogeneous and is classified as subgrid convective precipitation. All the precipitation that are not classified as subgrid convective precipitation are put in the resolved precipitation category. We have tested the sensitivity of the "3 times" assumption using 2 times and 4 times the subdomain-averaged value as the threshold. We found the partitioned subgrid convective and resolved precipitation insensitive to this parameter. All the subgrid convective and resolved precipitation are then summed up in the subdomain and averaged by the number of CRM grid points in the subdomain to get subdomain-averaged values. This subdomain-averaged subgrid convective precipitation is referred to as convective precipitation hereafter and then compared with the convective precipitation predicted by the ZM scheme at various resolutions.

3. Results

3.1. Resolution Adaptability of Convective Transport of MSE

Figure 3 shows the convective, resolved, and total transport of MSE from the three sets of ZM experiments and the CRM simulation described in section 2.2. Ideally, when model resolution increases, the total vertical transport of MSE in the analysis domain should be the same, while convective transport should decrease with higher resolution and the resolved transport increases. That is the case for the CRM results, because the same simulation output is analyzed as a function of the resolution. In the originalZM experiments, however, convective transport of MSE increases as the model resolution increases, and the increase is very significant. This confirms the results in Xiao15, which showed that the convective transport of MSE of the ZM scheme could increase as the resolution is increased if the spatial averaging method was not applied. More

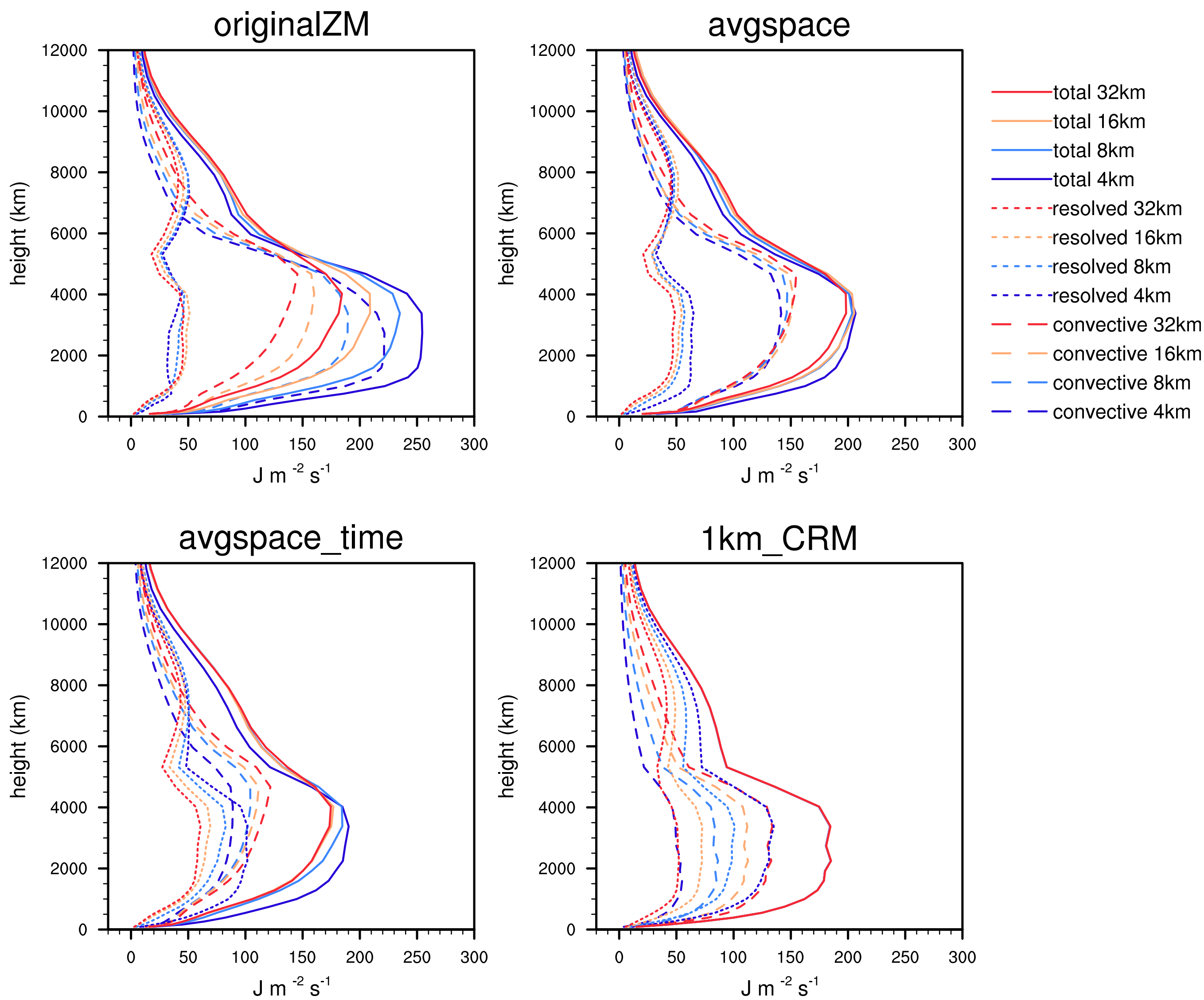

Figure 3. Total transport, resolved transport, and convective transport of MSE (J m^{-2} s^{-1}) for the three sets of experiments at 4, 8, 16, and 32 km grid spacings. The 1km_CRM profiles reflect the coarsened grids used for the subdomain calculations. The profiles are averaged over the analysis domain in space and the 136 h analysis period in time.

importantly, the total transport of MSE also increases as the resolution increases, driven by the increase in convective transport. Therefore, the total transport of MSE is not conserved across resolutions with the original ZM closure, suggesting double counting of vertical transport at high resolutions.

When spatial averaging of $(dA/dt)_{LS}$ is applied (i.e., avgspace experiments), a significant change is that the total transport of MSE is now almost independent of the resolution. The convective transport of MSE decreases slightly as the resolution becomes higher, instead of increasing as in the originalZM experiments. This reaffirms the results from in Xiao15 that the spatial averaging of $(dA/dt)_{LS}$ improves the resolution adaptability of the ZM scheme. When temporal averaging is additionally applied (i.e., avgspace_time experiments), the resolution adaptability is further improved. For example, the reduction of convective transport of MSE from 32 to 4 km grid spacing is bigger compared to that from the avgspace experiments. The resolved transport of MSE from the 4 km grid spacing simulation is almost doubled compared to the 32 km grid spacing simulation, which is a bigger increase than in the avgspace experiments.

Figure 4 shows the convective transport fraction, which is calculated as the ratio of the convective transport of MSE to the total transport of MSE. As expected from the CRM simulation, this convective transport

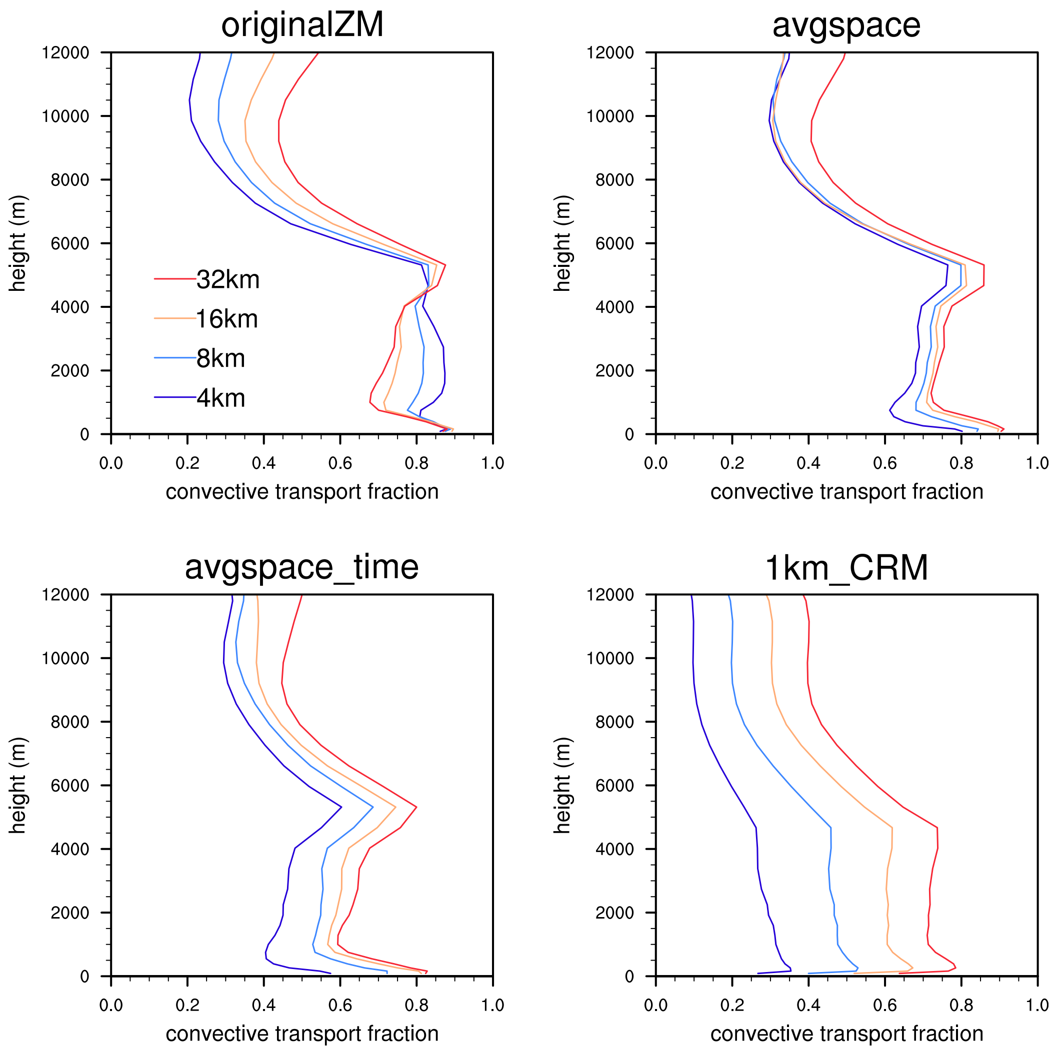

Figure 4. The fraction of convective transport of MSE over the total transport of MSE for the three sets of experiments performed with 4, 8, 16, and 32 km grid spacings. The 1km_CRM profiles represent the diagnosed convective transport fraction for the coarsened subdomains. Values are averaged over the analysis domain in space and the 136 h analysis period in time.

fraction decreases significantly as the resolution increases. However, in the originalZM runs, between 1 and 5 km heights, the convective transport fraction increases with the increase of resolution, which is the opposite of the CRM results (Figures 4a and 4d). With the spatial averaging of $(dA/dt)_{LS}$, the trend reverses at all vertical levels. When the temporal averaging is further applied, the reduction of convective transport fraction with the increase of resolution is more pronounced, although it is still less than that of the CRM diagnosis. The difference in the profile shape near the surface between the CRM results and the ZM simulations is possibly due to large convective transport of MSE near the surface in the ZM experiments.

Figure 5 more clearly shows the improved resolution adaptability due to the averaging methods. The decrease of convective transport of MSE is about 60% from 32 to 4 km grid spacing in the CRM simulation. In the originalZM simulations, convective transport of MSE increases by about 20% from 32 to 4 km grid spacing. Spatial averaging improves the resolution dependence, leading to a 15% decrease of convective transport of MSE in avgspace. Temporal averaging further improves the result, with a decrease of convective transport of MSE of about 30% in avgspace_time. Total transport of MSE increases by about 20% in the originalZM simulations, but is reasonably conserved with spatial and temporal averaging in the avgspace and avgspace_time sets of experiments.

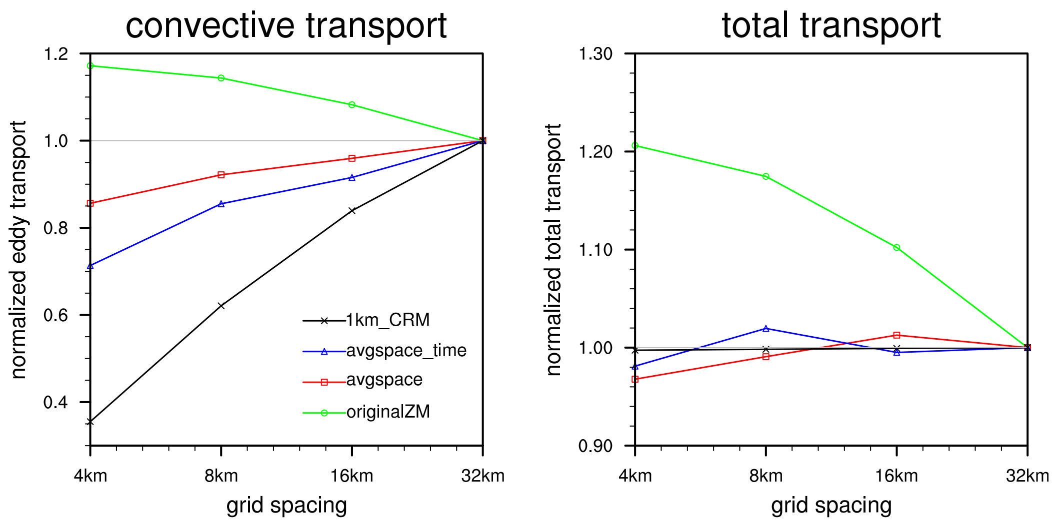

Figure 5. Resolution dependence of convective and total transport of MSE at a height of 4.7 km elevation (the level with the largest convective transport of MSE). The values for different grid spacings are normalized by the value at 32 km grid spacing. The grey line is at 1.0 to help guide the eye.

The resolution adaptability of convective mass flux (updraft only) is similar to that of convective transport of MSE (Figure 6). The implication of this is that the cloud-base mass flux, M_b, is the primary driver of the resolution dependence of both convective transport of MSE and convective mass flux. The M_b behavior in turn is dictated by $(dA/dt)_{LS+}$ as shown theoretically in equation (5).

Comparing with the offline results in Xiao15, from 32 to 8 km grid spacing, they found a 30% decrease in convective transport of MSE using the ZM scheme with spatial averaging, while the online result in this study (avgspace_time) shows a 15% decrease for the same change in grid spacing. We also notice that the underestimation of the mean magnitude of convective transport of MSE by ZM in the offline diagnosis of Xiao15 ($\sim$50%) seems much less pronounced (see Figure 3). These differences could be partially attributed to the coupling in the fully interactive model. In the offline test, the ZM scheme is responding to $(dA/dt)_{LS}$ diagnosed from a pre-existing CRM simulation, thus convective transport of MSE calculated from ZM does not feed back to the simulation. In the fully interactive model, however, the relationship between the parameterized convection and its grid-scale environment can be complicated by feedbacks involving numerical noise in resolved dynamics (Lander & Hoskins, 1997; Skamarock, 2004), the lack of resolution adaptability of other physics schemes, and the impact of other deficiencies in the convection parameterization (Gustafson et al., 2013). However, the effect of spatial and temporal averaging is still evident despite the complicated interactions in the fully interactive model.

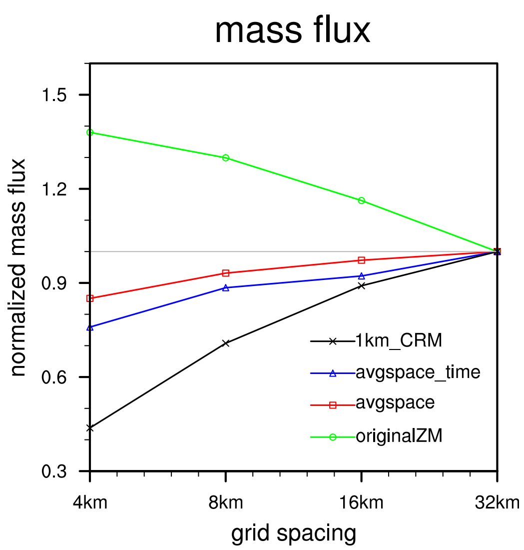

Figure 6. Same as Figure 5, but for updraft mass flux at 4.7 km normalized by the value at 32 km grid spacing.

To illustrate why applying spatial and temporal averaging improves the scheme's performance at higher resolutions, we analyzed the frequency distribution of $(dA/dt)_{LS}$ at 4 km grid spacing for a 2 h period with heavy precipitation within a monsoon event for three different setups: no averaging, spatial averaging, and spatial-temporal averaging (Figure 7). Comparing the three approaches, we see that applying spatial averaging significantly reduces the spread of $(dA/dt)_{LS}$ and temporal averaging further reduces it. With this reduction of spread, the difference between the spatiotemporal averages of $(dA/dt)_{LS+}$ and $(dA/dt)_{LS}$ (a positive value for the period under consideration) decreases because the probability of negative values is reduced. (The probabilities of negative $(dA/dt)_{LS}$ are 27.1%, 23.4%, and 19.5%, for

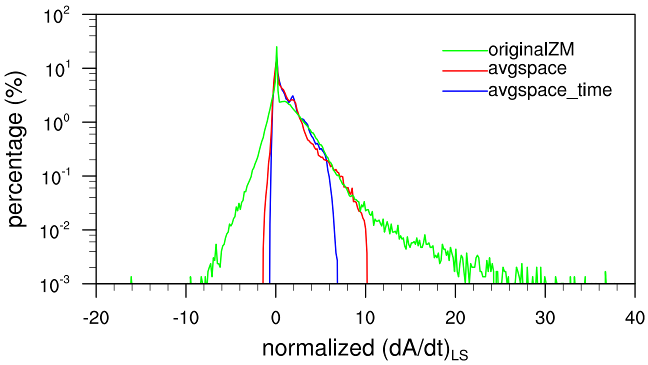

Figure 7. PDF of $(dA/dt)_{LS}$ from the 4 km grid spacing simulations for a 2 h monsoon period beginning at 23 January 2006 00:00 UTC. The values are normalized by the mean from the analysis area averaged during the 2 h.

originalZM, avgspace, and avgspace_time, respectively, during the 2 h period) Given that (1) $(dA/dt)_{LS+}$ dictates the resolution dependence of convective transport of MSE and (2) $(dA/dt)_{LS}$ is shown to have good resolution dependence in terms of spatiotemporal average, this decrease in the difference between the two leads to improved resolution dependence of convective transport of MSE. However, the spatial and temporal averaging also lead to more frequent convection triggering during this period. This overprediction of convective frequency is more pronounced at higher resolutions. We will further discuss the consequence of this overprediction in section 3.3.

3.2. Resolution Adaptability of Precipitation

The convective, resolved, and total precipitation from the CRM diagnosis and the three sets of experiments are shown in Figure 8. The diagnosed convective and resolved precipitation from the 1km_CRM simulation mostly agrees with the results for convective and resolved transport of MSE in terms of resolution dependence. At 4 km grid spacing, the convective precipitation is much smaller than the resolved part. The convective precipitation fraction increases significantly when the grid spacing increases. At 16 km grid spacing, the convective precipitation becomes larger than the resolved precipitation for the 1km_CRM benchmark simulation. This is also the case in convective and resolved transport of MSE (Figure 3). This means the method used to diagnose convective and resolved precipitation from the CRM could be used as an additional evaluation of the resolution dependence of the ZM experiments that takes a more integrated view across all the processes in the model contributing to precipitation.

Like convective transport of MSE, the convective precipitation in the originalZM experiments is larger at higher resolutions, and total precipitation is not conserved. However, when the spatial averaging of $(dA/dt)_{LS}$ is applied, there is a clear decreasing trend of convective precipitation with the increase of resolution, and a clear increasing trend of resolved precipitation. More importantly, the total precipitation is now relatively conserved across the analyzed grid spacings. When both the spatial and temporal averaging of $(dA/dt)_{LS}$ are applied (avgspace_time), the resolution adaptability is closest to the CRM simulation. One notable improvement with the additional temporal averaging of $(dA/dt)_{LS}$ is that the convective precipitation is smaller than resolved precipitation at 4 and 8 km grid spacings. This is consistent with the CRM diagnosis. In the originalZM and avgspace sets of experiments, convective precipitation is always larger than resolved precipitation at all resolutions.

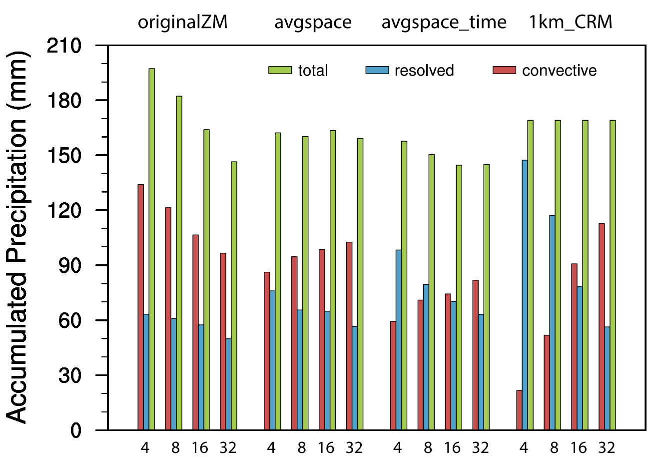

Figure 8. Precipitation partition change among convective, resolved, and total precipitation categories as a function of grid spacing. The numbers on the horizontal axis represent the grid spacing (km) of the simulations. The precipitation is accumulated over the analysis period and averaged for the analysis domain.

3.3. Spatial and Temporal Distributions of Precipitation

Ideally the overall strength of parameterized convection should decrease with higher resolution, and the relative fluctuations about the mean should increase (Plant & Craig, 2008), which implies less frequent convection and stronger extremes at higher resolutions. The spatial and temporal averaging algorithms proposed here are designed to improve the resolution-dependent behavior of the mean strength of parameterized convection only. As shown in Figure 7, such spatial and temporal averaging reduce the variability of $(dA/dt)_{LS}$, which is directly related to cloud-base mass flux (equation (5)), i.e., the parameterized convection strength. There is also a tendency toward more pronounced overprediction of convection frequency, especially at high resolutions.

With these issues in mind, we examine the impact of spatial and temporal averaging on the spatial and temporal distributions of precipitation at 4 km grid spacing. As Figure 9 shows, the spatial pattern of convective precipitation dominates that of total precipitation in originalZM. The convective precipitation shows larger spatial variability than avgspace and avgspace_time, but the mean magnitude of the

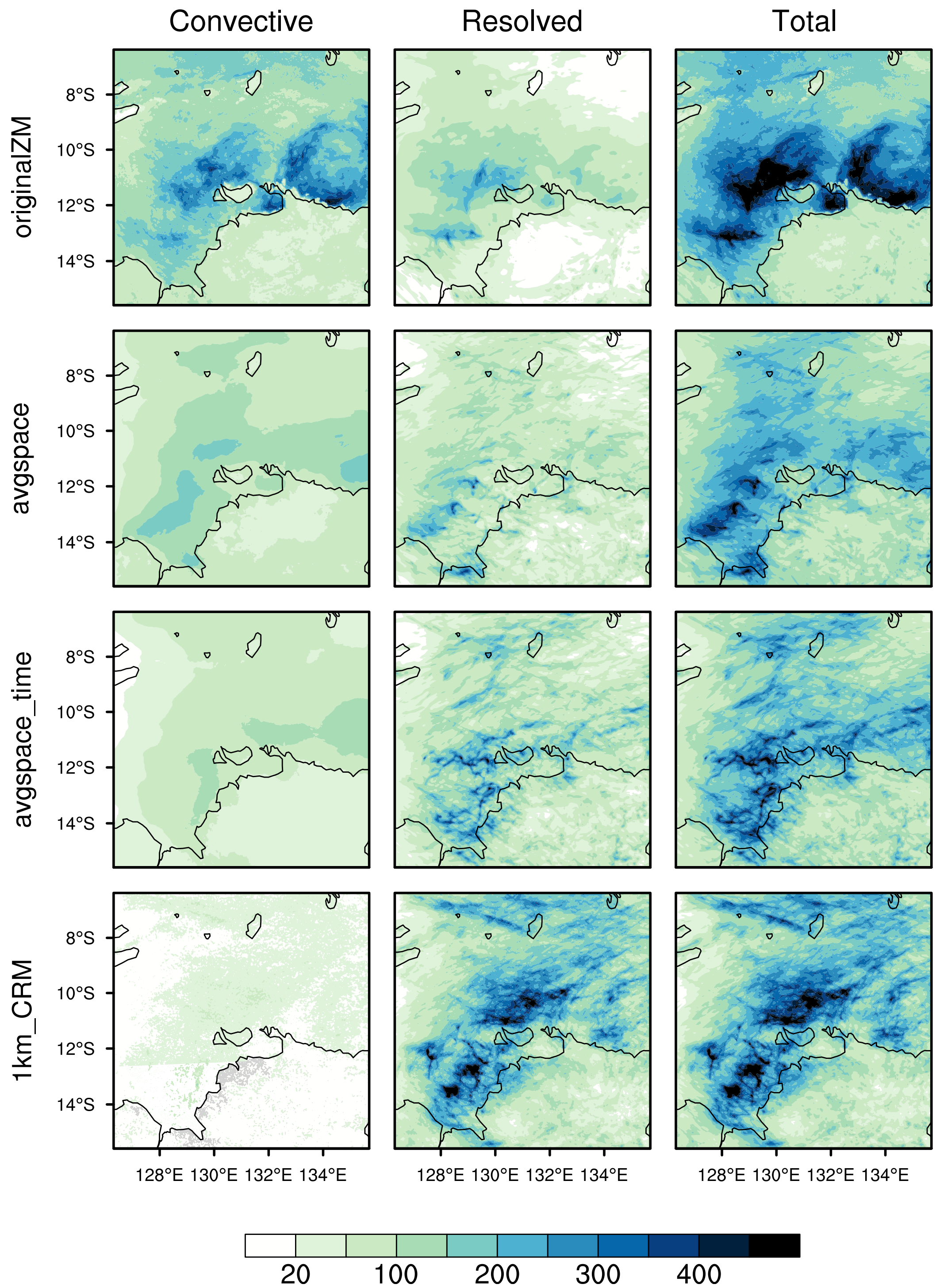

Figure 9. Accumulated convective, resolved, and total precipitation (mm) for the 4 km grid spacing simulations from the three sets of experiments and 1km_CRM. The precipitation is accumulated over the analysis period. Plots in the same column are for the same precipitation type, while plots in the same row are for the same experiment. Experiment names are shown on the left-hand side of each row.

convective precipitation is too strong and the spatial pattern is also quite different from the pattern diagnosed from the 1km_CRM simulation. After spatial and temporal averaging, convective precipitation becomes weaker and resolved precipitation strengthens. The total precipitation pattern in the averaging experiments becomes dominated by the pattern of resolved precipitation. Despite the smoothing introduced by our averaging method on the convective precipitation, the resolved precipitation pattern seems to contain more small-scale variations in avgspace and avgspace_time, which leads to a more realistic-looking total precipitation pattern. We also compared the spatial distribution of precipitation of the 8 km grid spacing (Figure 10) and 16 km grid spacing (Figure 11) simulations. For both grid spacings, the results

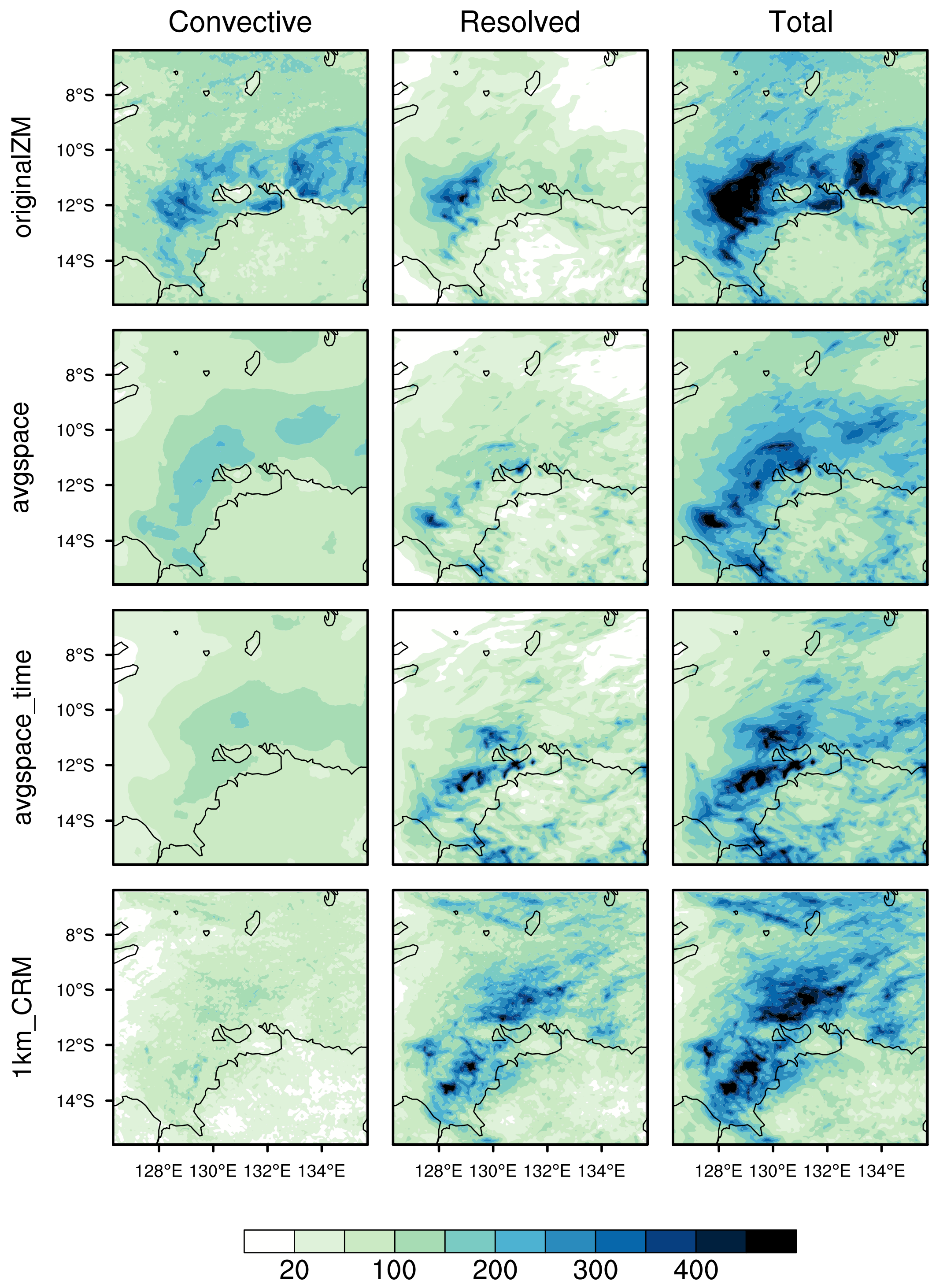

Figure 10. Same as Figure 9, but for 8 km grid spacing simulations.

are similar to the 4 km grid spacing results; except for the 16 km grid spacing simulation where the overprediction of convective precipitation by the originalZM simulation is not very significant.

On the instantaneous precipitation plot with 4 km grid spacing (Figure 12), we can see the smoothing of instantaneous convective precipitation with the averaging algorithms as expected. It also clearly shows the improved small-scale variations in the instantaneous resolved precipitation with the averaging algorithms,

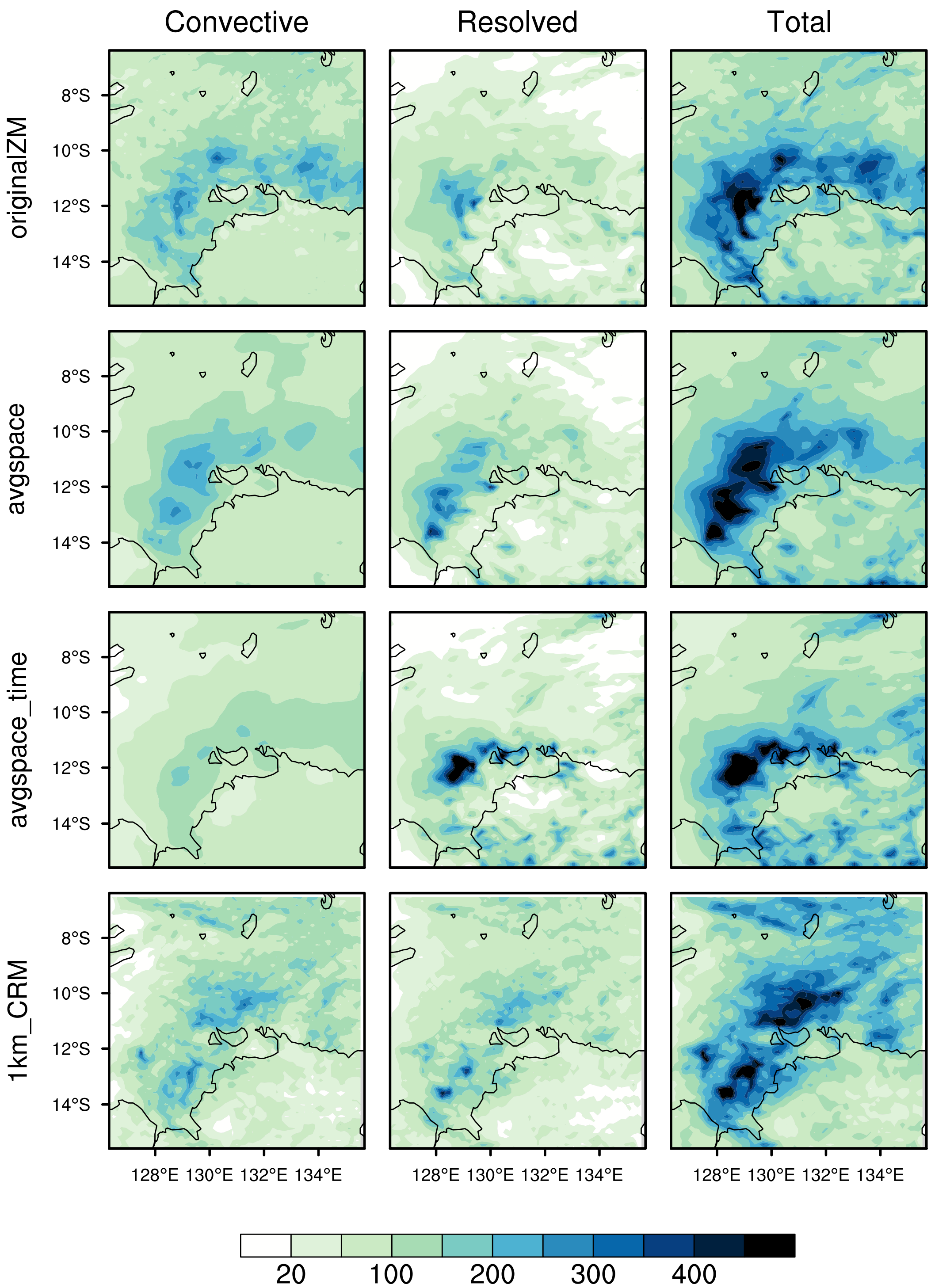

Figure 11. Same as Figure 9, but for 16 km grid spacing simulations.

for example, the rain bands to the northeast of the domain, which is simulated better in avgspace than originalZM, and even better in avgspace_time, compared to CRM results. Thus the smoothing of instantaneous convective precipitation does not deteriorate but improves the simulation of instantaneous total precipitation.

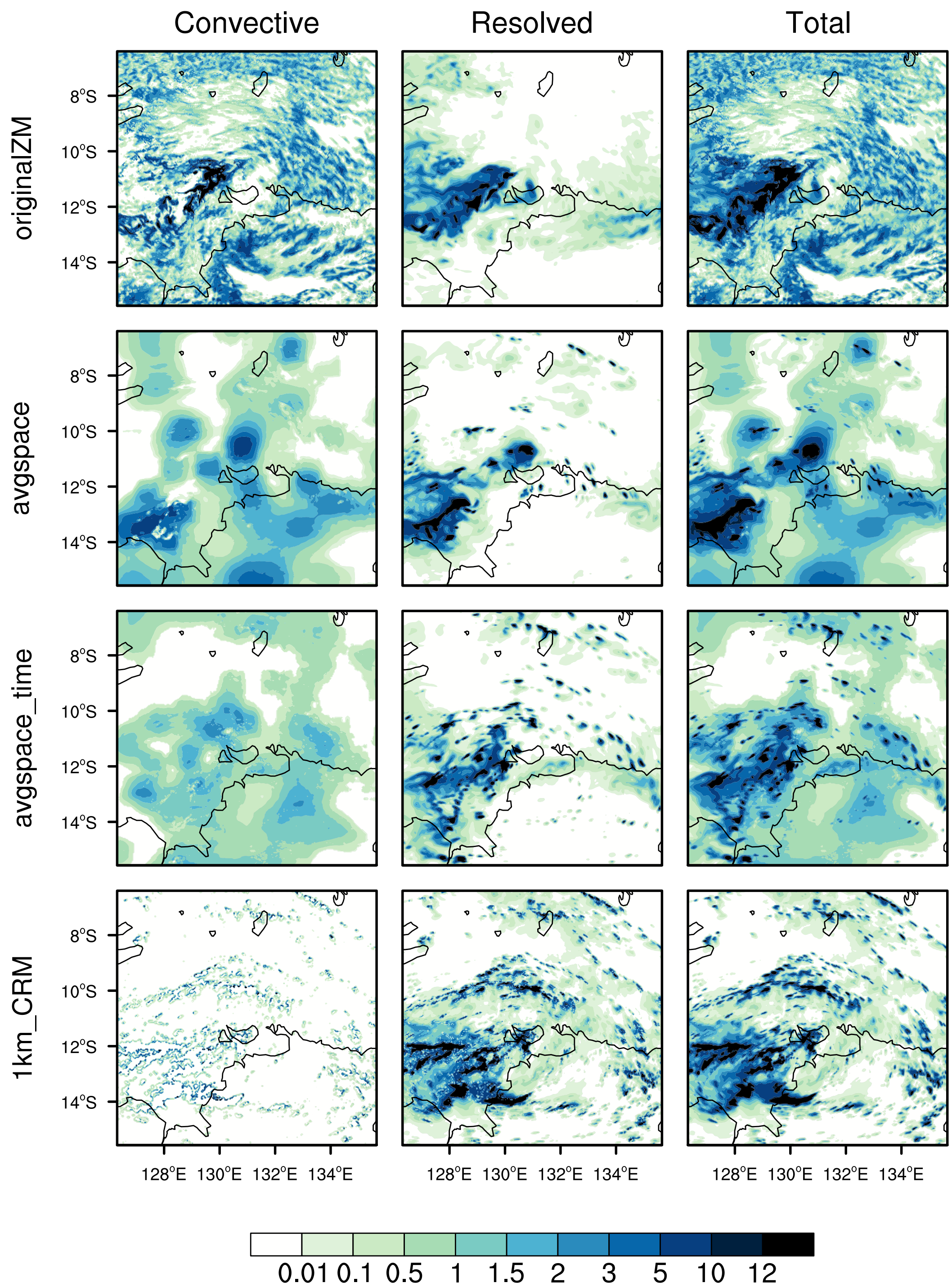

Figure 12. Instantaneous precipitation (mm h^{-1}) at 24 January 04:00 for the 4 km grid spacing simulations from each experiment and 1km_CRM.

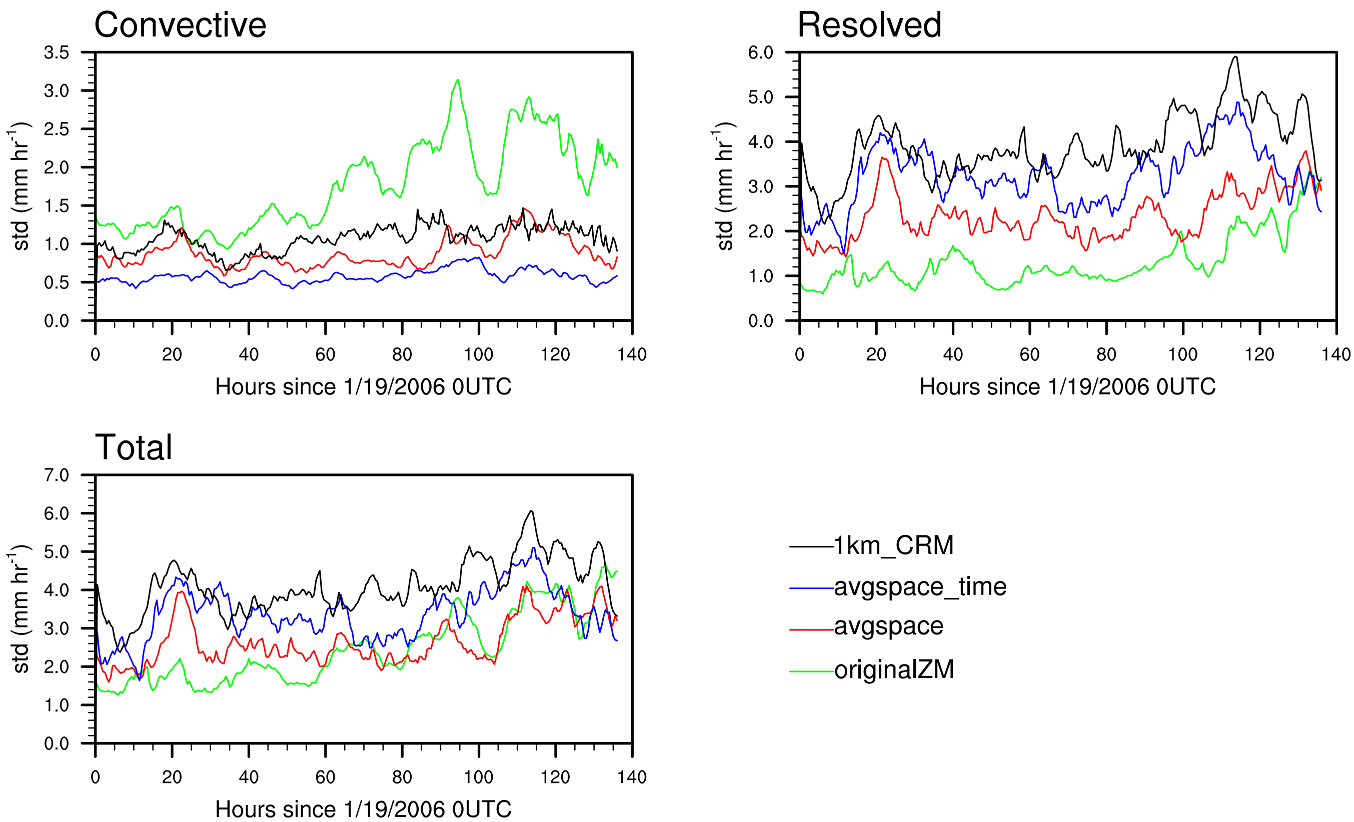

Figure 13. Time series of standard deviation for spatial variations of convective, resolved, and total precipitation (mm h^{-1}) for the 4 km grid spacing simulations from each experiment.

Taking a closer look at precipitation variability, the standard deviation for spatial variations of convective precipitation is overpredicted by the originalZM simulation (Figure 13). The averaging algorithms reduce the standard deviation to slightly smaller than that of the CRM results. In comparison, the standard deviation of resolved precipitation increases with spatial averaging, and increases further with spatiotemporal averaging. The standard deviation of total precipitation simulated by avgspace_time is the closest one compared to CRM results. The simulated time series of precipitation also looks more realistic with our averaging algorithms (Figure 14): the total amount improves and the timing of the synoptic-scale averaged precipitation is much better. From these results, it seems that we can improve the spatial and temporal distributions of total precipitation at high resolutions just by reducing the mean strength of convective precipitation with the averaging method.

The most likely reason for the improved precipitation distribution with the averaging methods is that by reducing the convective precipitation amount, more moisture is left in the column to allow for interactions between resolved dynamics and microphysics, which leads to enhanced fine-scale details, both in space and time. If, in addition to improving the mean strength of parameterized convection, we can also improve the representation of the variability of convective transport of MSE with either a stochastic (Wang et al., 2016) or a better deterministic scheme, we may see further improvements in the partition between convective and resolved precipitation and in the simulation of overall precipitation distribution.

4. Summary and Discussions

Applying a QE-based convection parameterization directly at high resolutions violates the presumptions of the QE hypothesis and masks the resolution adaptability of QE-based closures, which comes with the

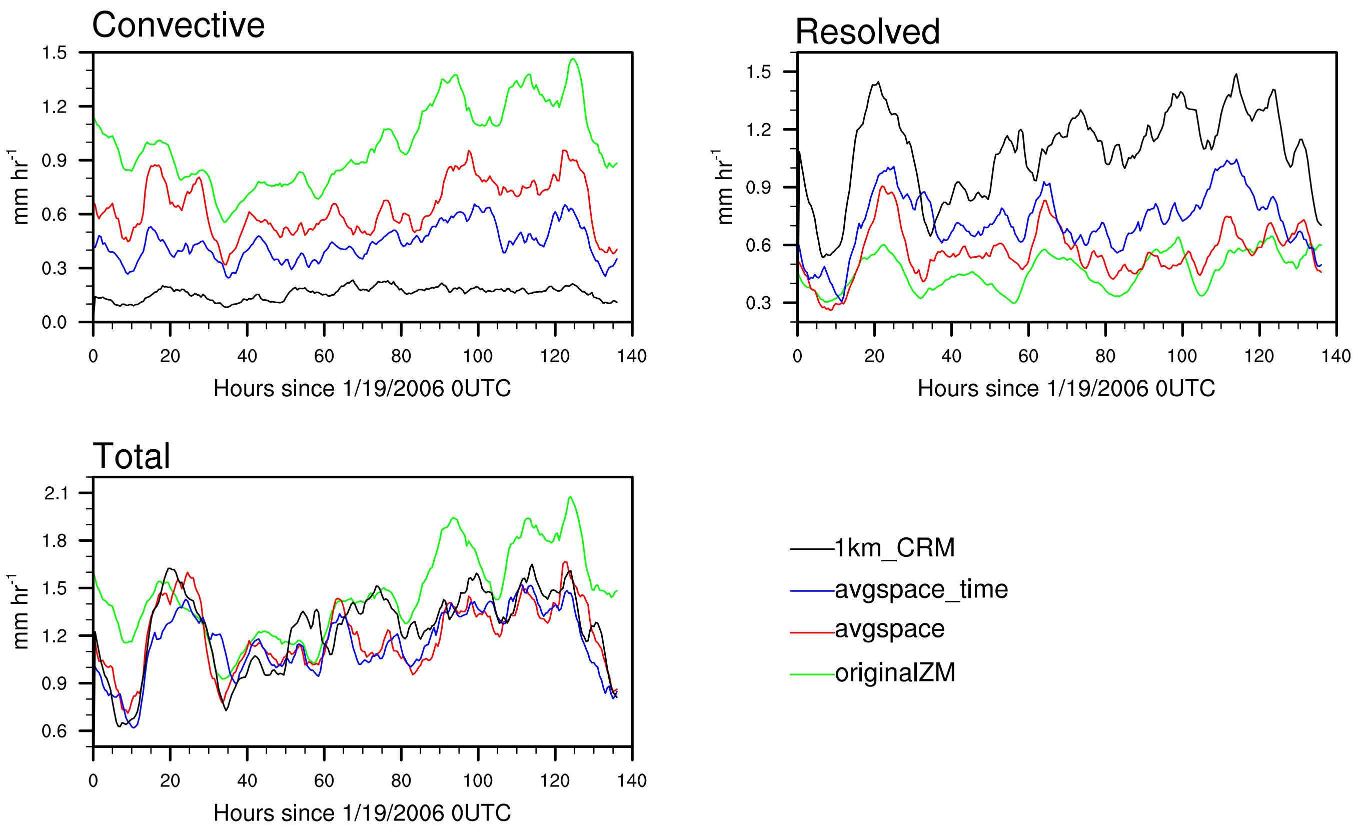

Figure 14. Time series of domain mean convective, resolved, and total precipitation (mm h^{-1}) for the 4 km grid spacing simulations from each experiment. Values are averaged over the analysis domain.

physically meaningful resolution dependence of grid-scale CAPE tendency, i.e., $(dA/dt)_{LS}$. In this study, we test spatial and temporal averaging algorithms for the grid-scale CAPE tendency calculation within the ZM scheme. Our algorithm allows for a consistent application of the QE-based closure regardless of model resolution. To evaluate the improvements in resolution adaptability, WRF model simulations with the original ZM scheme, the ZM scheme with spatial averaging, and the ZM scheme with both spatial and temporal averaging are performed with grid spacings varying from 4×4 to 32×32 km^2.

We show that the original ZM scheme has poor resolution adaptability, with the convective transport of MSE and convective precipitation both increasing significantly as the resolution increases. The total precipitation and total transport of MSE are also not conserved across resolutions. The spatial averaging method improves the resolution adaptability of the ZM scheme. Both the convective transport of MSE and convective precipitation show a decreasing trend as the resolution increases, and the total precipitation and total transport of MSE are nearly conserved for different resolutions. The spatiotemporal averaging experiments shows further improvements in resolution adaptability. The change of the magnitude and fraction of convective transport of MSE with resolution is closest to the benchmark CRM simulation for this methodology. The convective precipitation becomes smaller than resolved precipitation for grid spacings smaller than 8 km, which is consistent with the results from the CRM simulation.

We also examine the spatial and temporal distributions of precipitation, and show that even though the averaging methods tend to reduce the variability of parameterized convective transport and precipitation at small grid spacings, the reduction in the strength of parameterized convection leads to enhancement in both the mean and variability of resolved precipitation, which in turn leads to improved spatial and temporal distributions of total precipitation compared to the CRM benchmark.

In summary, we have shown that the methods presented in this study lead to improved performance of the ZM scheme at smaller grid spacings and are helpful for developing resolution adaptability for other cumulus parameterizations based on the QE assumption. It is possible that non-QE-based parameterizations can produce better resolution adaptability or better overall performance. The present work is meant to demonstrate the resolution adaptability that comes with consistent application of QE at high resolutions. As a next step, it is desirable to extend our methodology to prognostic closures like those of Pan and Randall (1998) and to test the impact of a resolution-adaptable stochastic formulation (e.g., Plant & Craig, 2008) together with the averaging algorithms.

Acknowledgments

Support for this work was provided by Scientific Discovery through Advanced Computing (SciDAC) program funded by the U.S. Department of Energy (DOE) Office of Advanced Scientific Computing Research and Office of Biological and Environmental Research. H.X. wishes to acknowledge the support from the Atmospheric System Research program funded by the U.S. Department of Energy (DOE) Office of Biological and Environmental Research. Y.Y. would also like to acknowledge funding from National Natural Science Foundation of China 91437101. The authors would like to thank Balwinder Singh, Zhe Feng, Hui Wan, Xiaoliang Song, Samson M. Hagos, Chun Zhao, and Qing Yang for their help and valuable discussions. The simulations are performed at National Energy Research Scientific Computing Center (NERSC). NCEP FNL Operational Model Global Tropospheric Analysis were obtained from National Centers for Environmental Prediction/National Weather Service/NOAA/U.S. Department of Commerce (2000), https://doi.org/10.5065/D6M043C6. TRMM precipitation data were obtained from NASA Goddard Space Flight Center, https://pmm.nasa.gov/trmm.

References

Arakawa, A. (2004). The cumulus parameterization problem: Past, present, and future. *Journal of Climate*, *17*(13), 2493–2525. https://doi.org/10.1175/1520-0442(2004)017<2493:Ratcpp>2.0.Co;2

Arakawa, A., & Jung, J. H. (2011). Multiscale modeling of the moist-convective atmosphere—A review. *Atmospheric Research*, *102*(3), 263–285. https://doi.org/10.1016/j.atmosres.2011.08.009

Arakawa, A., & Schubert, S. (1974). Interactions of a cumulus cloud ensemble with the large-scale environment, Part I. *Journal of the Atmospheric Sciences*, *31*, 674–701. https://doi.org/10.1175/1520-0469(1974)031<0674:IOACCE>2.0.CO;2

Arakawa, A., & Wu, C.-M. (2013). A unified representation of deep moist convection in numerical modeling of the atmosphere. Part I. *Journal of the Atmospheric Sciences*, *70*(7), 1977–1992. https://doi.org/10.1175/jas-d-12-0330.1

Bretherton, C. S., & Park, S. (2009). A new moist turbulence parameterization in the community atmosphere model. *Journal of Climate*, *22*(12), 3422–3448. https://doi.org/10.1175/2008jcli2556.1

Gerard, L., Piriou, J.-M., Brožková, R., Geleyn, J.-F., & Banciu, D. (2009). Cloud and precipitation parameterization in a meso-gamma-scale operational weather prediction model. *Monthly Weather Review*, *137*(11), 3960–3977. https://doi.org/10.1175/2009mwr2750.1

Grell, G. A., & Freitas, S. R. (2014). A scale and aerosol aware stochastic convective parameterization for weather and air quality modeling. *Atmospheric Chemistry and Physics*, *14*(10), 5233–5250. https://doi.org/10.5194/acp-14-5233-2014

Gustafson, W. I., Ma, P.-L., Xiao, H., Singh, B., Rasch, P. J., & Fast, J. D. (2013). The Separate Physics and Dynamics Experiment (SPADE) framework for determining resolution awareness: A case study of microphysics. *Journal of Geophysical Research: Atmospheres*, *118*, 9258–9276. https://doi.org/10.1002/jgrd.50711

Iacono, M. J., Mlawer, E. J., Clough, S. A., & Morcrette, J. J. (2000). Impact of an improved longwave radiation model, RRTM, on the energy budget and thermodynamic properties of the NCAR community climate model, CCM3. *Journal of Geophysical Research*, *105*(D11), 14873–14890. https://doi.org/10.1029/2000JD900091

Jones, T. R., & Randall, D. A. (2011). Quantifying the limits of convective parameterizations. *Journal of Geophysical Research*, *116*, D08210. https://doi.org/10.1029/2010JD014913

Kain, J. S., & Fritsch, J. M. (1990). A one-dimensional entraining detraining plume model and its application in convective parameterization. *Journal of the Atmospheric Sciences*, *47*(23), 2784–2802. https://doi.org/10.1175/1520-0469(1990)047<2784:aodepm>2.0.co;2

Lander, J., & Hoskins, B. J. (1997). Believable scales and parameterizations in a spectral transform model. *Monthly Weather Review*, *125*(2), 292–303. https://doi.org/10.1175/1520-0493(1997)125<0292:bsapia>2.0.co;2

Lee, S. S., Donner, L. J., Phillips, V. T. J., & Ming, Y. (2008). The dependence of aerosol effects on clouds and precipitation on cloud-system organization, shear and stability. *Journal of Geophysical Research*, *113*, D16202 https://doi.org/10.1029/2007JD009224

Liu, Y. C., Fan, J. W., Zhang, G. J., Xu, K. M., & Ghan, S. J. (2015). Improving representation of convective transport for scale-aware parameterization: 2. Analysis of cloud-resolving model simulations. *Journal of Geophysical Research: Atmospheres*, *120*, 3510–3532. https://doi.org/10.1002/2014JD022145

Ma, P. L., Rasch, P. J., Fast, J. D., Easter, R. C., Gustafson, W. I., Liu, X.,. . . Singh, B. (2014). Assessing the CAM5 physics suite in the WRF-Chem model: Implementation, resolution sensitivity, and a first evaluation for a regional case study. *Geoscientific Model Development*, *7*(3), 755–778. https://doi.org/10.5194/gmd-7-755-2014

Mapes, B. E. (1997). Equilibrium vs. activation controls on large-scale variations of tropical deep convection. In R. K. Smith (Ed.), *The physics and parameterization of moist atmospheric convection* (pp. 321–358). Dordrecht, Netherlands: Kluwer Academic.

May, P. T., Allen, G., Vaughan, G., & Connolly, P. (2009). Aerosol and thermodynamic effects on tropical cloud systems during TWPICE and ACTIVE. *Atmospheric Chemistry and Physics*, *9*(1), 15–24. https://doi.org/10.5194/acp-9-15-2009

Moorthi, S., & Suarez, M. J. (1992). Relaxed Arakawa-Schubert—A parameterization of moist convection for general-circulation models. *Monthly Weather Review*, *120*(6), 978–1002. https://doi.org/10.1175/1520-0493(1992)120<0978:rasapo>2.0.co;2

Morrison, H., Curry, J. A., & Khvorostyanov, V. I. (2005). A new double-moment microphysics parameterization for application in cloud and climate models. Part I: Description. *Journal of the Atmospheric Sciences*, *62*(6), 1665–1677. https://doi.org/10.1175/Jas3446.1

Neelin, J. D., Peters, O., Lin, J. W., Hales, K., & Holloway, C. E. (2008). Rethinking convective quasi-equilibrium: Observational constraints for stochastic convective schemes in climate models. *Philosophical Transactions of the Royal Society A*, *366*(1875), 2581–2604. https://doi.org/10.1098/rsta.2008.0056

Pan, D.-M., & Randall, D. D. A. (1998). A cumulus parameterization with a prognostic closure. *Quarterly Journal of the Royal Meteorological Society*, *124*(547), 949–981. https://doi.org/10.1002/qj.49712454714

Park, S. (2014). A Unified Convection Scheme (UNICON). Part I: Formulation. *Journal of the Atmospheric Sciences*, *71*(11), 3902–3930. https://doi.org/10.1175/jas-d-13-0233.1

Plant, R. S., & Craig, G. C. (2008). A stochastic parameterization for deep convection based on equilibrium statistics. *Journal of the Atmospheric Sciences*, *65*(1), 87–105. https://doi.org/10.1175/2007jas2263.1

Raymond, D. J., & Herman, M. J. (2011). Convective quasi-equilibrium reconsidered. *Journal of Advances in Modeling Earth Systems*, *3*, M08003. https://doi.org/10.1029/2011MS000079

Skamarock, W. C. (2004). Evaluating mesoscale NWP models using kinetic energy spectra. *Monthly Weather Review*, *132*, 3019–3032. https://doi.org/10.1175/MWR2830.1

Steiner, M., Houze, R. A., & Yuter, S. E. (1995). Climatological characterization of 3-dimensional storm structure from operational radar and rain-gauge data. *Journal of Applied Meteorology*, *34*(9), 1978–2007. https://doi.org/10.1175/1520-0450(1995)034<1978:ccotds>2.0.co;2

Tao, W.-K. (2007). Cloud resolving Modeling. *Journal of the Meteorological Society of Japan*, *85B*, 305–330. https://doi.org/10.2151/jmsj.85B.305

Wang, Y., Zhang, G. J., & Craig, G. C. (2016). Stochastic convective parameterization improving the simulation of tropical precipitation variability in the NCAR CAM5. *Geophysical Research Letters*, *43*, 6612–6619. https://doi.org/10.1002/2016GL069818

Williams, P. D. (2005). Modelling climate change: The role of unresolved processes. *Philosophical Transactions of the Royal Society A*, *363*(1837), 2931–2946. https://doi.org/10.1098/rsta.2005.1676

Xiao, H., Gustafson, W. I., Hagos, S. M., Wu, C.-M., & Wan, H. (2015). Resolution-dependent behavior of subgrid-scale vertical transport in Zhang-McFarlane convection parameterization. *Journal of Advances in Modeling Earth Systems*, *7*, 537–550. https://doi.org/10.1002/2014MS000356

Yano, J. I., & Plant, R. S. (2012). Convective quasi-equilibrium. *Reviews of Geophysics*, *50*, RG4004. https://doi.org/10.1029/2011RG000378

Zhang, G. J. (2002). Convective quasi-equilibrium in midlatitude continental environment and its effect on convective parameterization. *Journal of Geophysical Research*, *107*(D14), 4220. https://doi.org/10.1029/2001JD001005

Zhang, G. J. (2003). Convective quasi-equilibrium in the tropical western Pacific: Comparison with midlatitude continental environment. *Journal of Geophysical Research*, *108*(D19), 4592. https://doi.org/10.1029/2003JD003520

Zhang, G. J., Fan, J. W., & Xu, K. M. (2015). Comments on "A unified representation of deep moist convection in numerical modeling of the atmosphere. Part I. *Journal of the Atmospheric Sciences*, *72*, 2562–2565. https://doi.org/10.1175/jas-d-14-0246.1

Zhang, G. J., & McFarlane, N. A. (1995). Sensitivity of climate simulations to the parameterization of cumulus convection in the Canadian climate center general-circulation model. *Atmosphere-Ocean*, *33*(3), 407–446.